PolyJet-Based 3D Printing against Micromolds to Produce Channel Structures for Microchip Electrophoresis

Major A. Selemani, Andre D. Castiaux, and R. Scott Martin*

ACCESS | Metrics & More | Article Recommendations | Supporting Information

ABSTRACT: In this work, we demonstrate the ability to use micromolds along with a stacked three-dimensional (3D) printing process on a commercially available PolyJet printer to fabricate microchip electrophoresis devices that have a T-intersection, with channel cross sections as small as 48×12 μm^2 being possible. The fabrication process involves embedding removable materials or molds during the printing process, with various molds being possible (wires, brass molds, PDMS molds, or sacrificial materials). When the molds are delaminated/removed, recessed features complementary to the molds are left in the 3D prints. A thermal lab press is used to bond the microchannel layer that also contains printed reservoirs against another solid 3D-printed part to completely seal the microchannels. The devices exhibited cathodic electroosmotic flow (EOF), and mixtures of fluorescein isothiocyanate isomer I (FITC)-labeled amino acids were successfully separated on these 3D-printed devices using both gated and pinched electrokinetic injections.

Device on 3D printed on mold

While this application is focused on microchip electrophoresis, the ability to 3D-print against molds that can subsequently be removed is a general methodology to decrease the channel size for other applications as well as to possibly integrate 3D printing with other production processes.
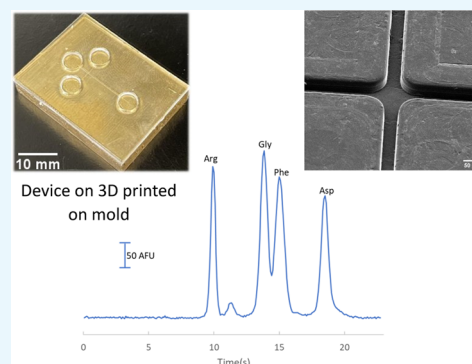
■ INTRODUCTION

Microchip electrophoresis has been widely shown to be an attractive separation technique for a wide range of applications including environmental monitoring, biomedical and pharmaceutical analysis, forensics investigation, and clinical diagnostics.[1−4] Such devices are characterized by their ability to analyze small quantities of a sample with small reagent consumption, reduced analysis time, and in some instances lower limits of detection.[5−7] Several materials have been used for fabrication since microchip electrophoresis devices were first proposed by Manz et al.[8] Initial approaches involved the use of photolithography and wet etching to fabricate devices in glass substrates (after thermal bonding against a cover), with channel dimensions of ~30×10 μm^2.[9] Glass was initially a popular material owing to its surface similarities to fused-silica capillaries, high thermal stability, biocompatibility, chemical resistance, optical transparency, and stable electroosmotic flow (EOF).[10,11] Despite the benefits of using glass for microdevice fabrication, the overall process is often expensive, time consuming, uses hazardous chemicals (such as HF), and requires a clean room facility.[12]

Several polymer approaches can be used as an alternative to glass for the rapid prototyping of microchip devices. Injection molding or hot embossing against molds of the design of interest can ensure mass production of polymer devices using relatively expensive setups.[13,14] Whitesides introduced the use of cross-linked elastomeric polymer, poly(dimethylsiloxane) (PDMS), as a substrate in microchip fabrication via soft lithography.[15,16]

The material has become popular due to the low cost and ease of fabrication as well as its gas permeability and cell biocompatibility. In addition, the adhesive and optical transparent nature of PDMS allows integration to other substrates including glass and rigid polymers with reversible or irreversible bonding.[16,17] Disadvantages of using PDMS devices include the need to fabricate the master in a clean environment and issues with scaling the technology for mass production. In addition, the hydrophobic nature of PDMS can lead to adsorption issues (and less efficient separations) as well as EOF changes over time.[18,19]

Three-dimensional (3D) printing, also known as addictive manufacturing, has been shown to be a viable alternative for the fabrication of sophisticated microfluidic designs in a single printing step.[20−22] The time from initial design to final product is possible in a few hours per iteration. Moreover, most 3D printing technologies do not require a clean room facility, with other advantages including ease and uniformity of fabrication, file sharing between laboratories, and increased device-to-device reproducibility. Fused deposition modeling (FDM) has been the most popular 3D printing technique because of its ease and
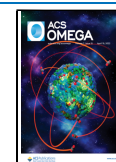
cost effectiveness. It has been used in microfluidics initially as a method of developing templates for PDMS devices fabricated from soft lithography.[23] FDM deposits liquefied thermoplastics extruded from a heated nozzle onto a surface platform layer-by-layer. Significant challenges exist with fabricating devices that are optically clear and liquid tight with the resolution needed to create true microchannels. Higher-resolution techniques include PolyJet and stereolithography (SLA) printing. For inkjet (i.e., Polyjet) 3D printing, devices are built by jetting photopolymer droplets onto a building tray and solidifying them with a UV light source (using acrylate-based materials and photoinitiators). A support material is used to fill enclosed microchannels, with mechanical removal after the printing process. Stereolithography (SLA) printing is gaining more interest in the fabrication of microfluidic devices because of its high resolution and limited postprocessing requirements. The technique involves focusing a laser on to a vat of photopolymer resin that chemically solidifies upon UV exposure. Post processing involves the removal of unpolymerized resin liquid from the interior channels.

Several research groups have used these 3D printing technologies to fabricate complex microfluidic devices to analyze various chemical and biological samples.[24,25] However, fabrication of interior channels with commercial 3D printing systems is often limited to sub millifluidic range (300−1000 μm). Such millifluidic features are typically not suitable for high-performance microchip electrophoresis and other bioanalytical processes such as single-cell analysis. Breadmore et al. used a multimaterial FDM printing system to fabricate membrane-integrated devices with interior channels ($\sim$500 × 800 μm^2 cross section) for filtration and isotachophoresis of ampicillin.[22] Recently, Bahnemann et al. demonstrated a microfluidic free-flow electrophoresis technique to separate and concentrate amino acids.[25] The 3D-printed microchip devices had interior channels that were a cross section of 700 × 200 μm^2. As researchers continue to push for achievable feature sizes closer to printer resolution specifications as well as improving the overall printer resolution, the use of specially formulated resins in custom SLA printers has demonstrated that microchip devices with interior channels in the true microfluidic range can be fabricated.[26] Woolley et al. used such an approach to fabricate a 3D microfluidic device with channels (37 × 49 μm^2 cross section) for microchip electrophoresis separation of preterm birth biomarkers.[27] They also recently fabricated microchip electrophoresis devices containing spiral electrodes around the electrophoretic separation channel for capacitively coupled contactless conductivity detection.[28]

In this paper, we demonstrate the use of a commercial PolyJet printer to fabricate microfluidic devices with channel sizes <100 μm for microchip electrophoresis separation of fluorescently labeled amino acids. Embedding removable materials or molds along with a stacked printing process on a commercially available PolyJet 3D printer is used to fabricate microchannel networks. Devices are bonded against another 3D-printed part with a heated lab press. We show that various molds can be used (wires, brass molds, PDMS molds, or sacrificial materials) in the printing process. The bonded devices can support electrophoretic separations via gated or pinched injection schemes (cathodic EOF), with separation efficiencies similar to other polymer devices being possible.

◼ EXPERIMENTAL METHODS

Material and Chemicals. Veroclear-RGD810 print material and SUP706B support were purchased from Stratasys, Ltd.

(Eden Prairie, MN). Isopropyl alcohol was obtained from Thermo Fisher Scientific (St. Louis, MO). Nichrome wire, 0.025 and 0.05 mm diameters, was purchased from Alfa Aesar (Tewksbury, MA). Glycine, arginine, phenylalanine, aspartic acid, fluorescein isothiocyanate isomer I (FITC), N-cyclohexyl-3-aminopropanesulfonic acid (CAPS), and boric acid were purchased from Millipore Sigma-Aldrich (St. Louis, MO). N-160 Solvent thinner and carbon ink were purchased from Ercon Inc. (Wareham, MA). Poly(dimethylsiloxane) (PDMS) base and curing agent (Sylgard 184) were purchased from Dow Corning (West Salzburg, MI). Silicon wafer substrates were purchased from Empak Inc. (Arrowswest, CO). SU-50 and SU-8 developers were purchased from Kayaku Advanced Materials Inc. (Westborough, MA).

Fabrication of Molds. *Brass Mold.* A brass mold with raised structures was first designed in Autodesk Inventor Professional 2021 (Autodesk, Inc., San Rafael, CA). The CAD files were sent to the University of Kansas (Department of Physics Machine Shop and the NIBIB-funded Biotechnology Resource Center of Biomodular Multi-scale Systems for Precision Medicine), where high-precision micromilling was used to fabricate a 42 × 42 μm^2 positive relief microstructure in brass, as previously discussed.[29]

PDMS Mold. A negative (SU8-50) photoresist and a positive mask (with a simple T-structure) were used to fabricate 50 × 50 μm^2 recessed (negative relief) microstructures on a silicon wafer master.[30] The prepolymer PDMS was cast on the silicon master and cured in an oven at 55 °C for 2 h. The replica polymer mold with subsequent positive relief microstructure was then peeled from the master and used as a mold for printing.

Carbon Ink Mold. A positive relief master on a silicon wafer was fabricated using negative photoresist and a negative mask (with a simple T-structure). A PDMS mold was then fabricated on the silicon master using soft lithography. The micromolding in capillaries technique[30] was used to create carbon ink microstructures, by reversibly sealing the PDMS microchannels onto a glass substrate and filling with a 0.2% (w/v) carbon ink solution. The ink was dried in the oven at 85 °C for 4 h, after which time the PDMS mold was removed from the glass substrate, leaving a thin film of patterned carbon ink on the glass.[31,32]

PolyJet Printing. Devices were designed in Autodesk Inventor Professional 2021 and printed on a Stratasys J735 PolyJet 3D printer using their VeroClear material. VeroClear resin has been reported to contain isobornyl acrylate, acrylic monomer, acrylate oligomer, acrylic acid ester, and photoinitiator.[33,34] For the embedded wire technique, a stencil design model was first printed directly on the tray. A piece of glass was placed on top of the stencil with double-sided tape to secure the glass from moving during printing. Using the stencil as a guide, a section of nichrome wire was then placed on top of the glass and taped down on both ends. The print tray was dropped by the height of the glass, stencil, and outer diameter of the wire (with the previously described stacked printing process[24,35]). The designed model was then printed directly on top of the wire and glass. The total print time for all parts was 12 min in total. When the printing process was complete, the model was delaminated from the glass and the embedded wire was removed, leaving a recessed microchannel with dimensions of the outer diameter of the wire. Straight channel devices with 25 and 50 μm diameter channels were fabricated with the wire embedding technique.

PolyJet printing was also done against a positive relief structure made from brass, PDMS, or carbon ink. This was done by printing a stencil design model on the print tray and then
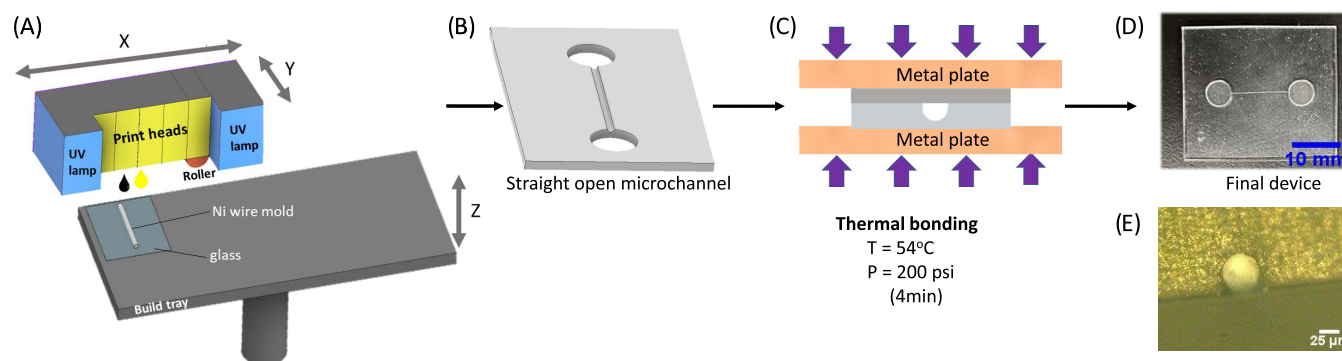
Figure 1. Fabrication of a straight microchannel device (25 or 50 μm diameter) with Polyjet 3D printing: (A) printing CAD design model direct on Ni wire of the desired dimension; (B) after removal of wire from the device; (C) thermal fusion bonding for sealing the channel; (D) photograph of the assembled device; and (E) bright-field micrograph showing the cross-sectional area of the sealed channel.

placing the mold on the stencil with double-sided tape. The print tray was dropped relative to the height of the stencil, mold, and structure. A device with reservoirs designed using Autodesk inventor Professional 2021 was then printed directly on top of the mold. For the brass and PDMS molds, after delaminating, the printed devices from the molds, the negative features created on the printed device were complementary to the positive features of the molds. The same brass and PDMS molds were used repeatedly throughout this work. For example, the same brass mold was used to print over 80 devices (and counting) and the same PDMS mold was utilized to print over 17 devices (and counting). For the carbon ink approach, after the printing process was completed, the carbon ink was transferred into the resulting print. The carbon ink was then removed in a postprocessing step using solvent thinner, leaving microchannels that match the dimensions of the carbon ink. Bright-field micrographs were taken with a Keyence VHX-500K digital microscope (Japan), and all channel measurements were done with VHX Measurement Software. Scanning electron microscopy (SEM) images were taken on high-resolution Inspect F50 (Thermo Fisher Scientific, Czech Republic). Depth profiles were measured using either a surface profiler (Dektak II, Vecco Instruments, Boston, MA) or a laser profiler (Keyence VK-9710K, Itasca, IL).

For all of these approaches, a thermal lab press (DABPRESS, Guangdong, China) was used to bond the microchannel layer with reservoirs against another solid 3D-printed part to completely seal the microchannels and create the final closed fluidic microchip. The overall device dimensions were 28×38 mm^2 ($W \times L$), and the reservoir radius was 2.5 mm. The bonding process, which took 4 min, was performed at 54 °C and 200 psi of pressure. The bonded devices were robust, with devices remaining bonded for up to 90 days of storage (longer times were not investigated).

Electrophoresis-Based Separations. Regardless of the mold that was used, each microchip device was treated with a corona discharge unit fitted with a fine tip electrode (model ETP BD-20, Electro-technic Products, Inc., Chicago, IL) before running the electrophoretic separations.[36] Boric acid buffer, either 25 and 10 mM (pH 10), was prepared in deionized water (18.0 MΩ cm). The electroosmotic flow (EOF) measurements on untreated and corona-treated straight channel devices were done using a boric acid buffer system (pH 10) and the current monitoring method described by Huang.[37] Briefly, the two reservoirs were filled with 25 mM boric acid buffer (pH 10), and one of the reservoirs was replaced by a reduced ionic strength

boric acid buffer of the same pH. The time required for the current to reach a constant level was recorded, and the EOF was calculated.[37] A similar process was used to determine the EOF at pH 11.2 using a CAPS buffer system. Ohm's law experiments were also done on 25 and 50 μm straight channel devices. The device channels were filled with boric acid buffer (25 mM, pH 10). High voltage was applied to one reservoir, and the other was grounded through a circuit that contained a 100 kΩ resistor. The voltage across this resistor was measured, and the electrophoretic current was calculated. A range of electrophoretic voltages were used (100−1200 V, glass high-voltage power supply).

Gated and pinched electrokinetic injection schemes were demonstrated in the separation of labeled amino acids on T-devices. For gated injections, samples were prepared in 20 mM boric acid buffer (pH 10). The amino acids glycine (Gly), arginine (Arg), phenylalanine (Phe), and aspartic acid (Asp) were labeled with fluorescein isothiocyanate isomer I (FITC) overnight at room temperature as previously discussed.[38] The device was placed on an inverted fluorescence microscope (Olympus IX71) fitted with a 10× objective (Olympus PLN2X. Japan). The sample reservoir was filled with a mixture of FITC-labeled amino acids, and buffer reservoir, buffer waste, and sample waste were filled with 20 mM boric acid buffer (pH 10). A LabSmith HVS448 3000 V high-voltage sequencer (Lab-Smith, Livermore, CA) with eight independent high-voltage (HV) channels was used as the electrophoresis voltage supply. The gated injection sequence for the brass and PDMS mold devices was accomplished by applying a high voltage (+410 V) to the buffer reservoir and a fraction of the high voltage (+400 V) to the sample reservoir, with sample waste and buffer waste grounded. Injections were achieved by floating the high voltage applied to the buffer reservoir for 2 s. For the carbon ink devices, the applied voltages at the sample reservoir and buffer reservoir were +200 and 210 V, respectively, and the injection time was 2 s. The detection window for brass, PDMS, and carbon ink mold devices was set at 0.70, 0.65, and 0.30 cm (distance from injection point), respectively. The resulting fluorescence signal was recorded with a QICam CCD digital camera (Q Imaging, British Columbia, Canada). The Supporting Information describes the use of a pinched injection process.

■ RESULTS AND DISCUSSION

PolyJet printers are a popular choice (along with SLA) for high-resolution 3D printing. This technique uses a waxylike sacrificial material to support interior features during printing. The
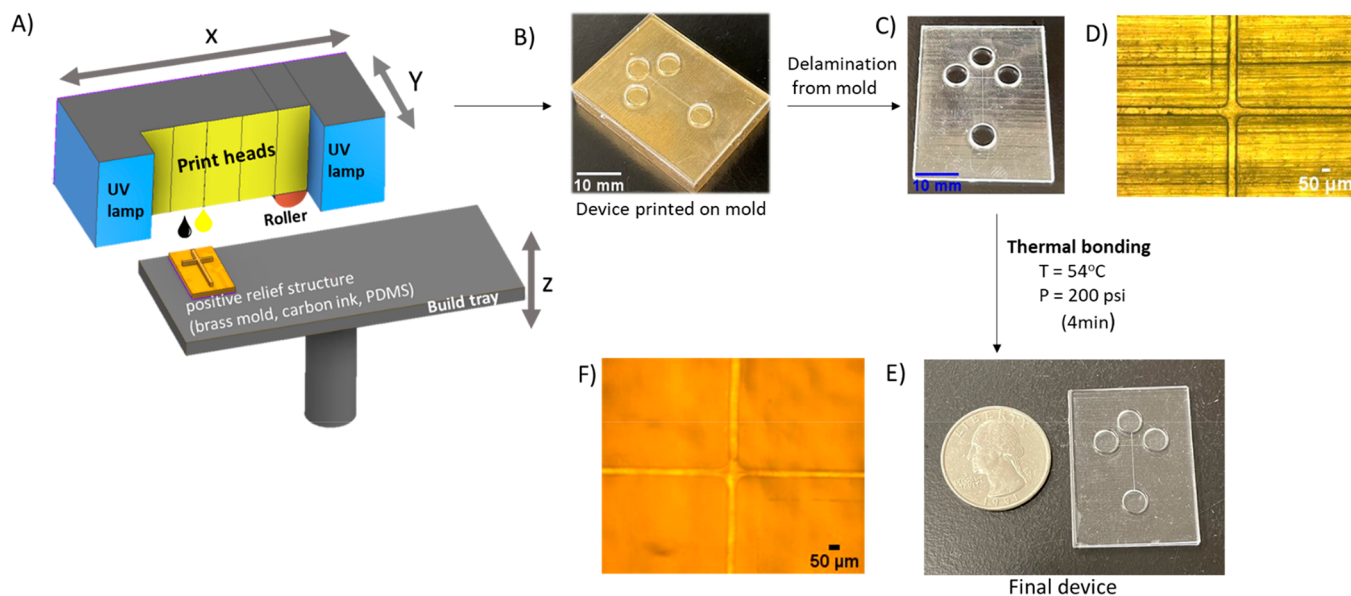
Figure 2. Fabrication of cross-channel structure with Polyjet 3D printer: (A) printing CAD design model on positive relief structure; (B) device printed on a brass mold; (C) device after delamination from mold; (D) bright-field micrograph of channel intersection before bonding; (E) bright-field micrograph of channel intersection after bonding; and (F) photograph of the final device (after bonding), with respect to a US quarter.

material is semisoluble in a caustic bath and requires some mechanical removal in post processing. This limits the channel sizes and complexity of the fluidic designs that can be fabricated (in our practice, channels smaller than 350 μm are very difficult to produce). Previously, our lab has demonstrated the use of a liquid support material in Polyjet printing using a stacked printing process, with the channel cross section being reduced to 200 × 200 μm^2, which is still too large for microchip-based electrophoresis.[35] Another possibility is printing open channels without utilizing support material; however, in our practice, this approach suffers from two limitations. First, our experiments in printing channels in this manner led to the resolution being limited to ~100 × 27 μm^2 and, second, the resulting print ends up with ridges on the top surface. When using thermal bonding against another 3D-printed part, these ridges led to incomplete bonding and leaking between the layers (Figure S1). One way around this limitation is to utilize nonprinted but removable materials (i.e., molds) on a flat surface to create open channels that can be subsequently bonded. Figure 1A shows the Polyjet stacked printing process that was developed to print over a straight nichrome wire mold placed on a glass surface. The microchannel on the 3D-printed part was complementary to the outer diameter (OD) of the nichrome wire. Straight channels as small as 25 μm were fabricated with this technique. Printing on the smooth glass surface created channels on the bottom side of the 3D print without any ridges on the surface to interfere with bonding. Initial experiments focused on determining optimal bonding conditions without collapsing the channel (using a heated lab press). We determined that a temperature of 54 °C and a pressure of 200 psi for 4 min yielded the most reproducible device sealing conditions. A photograph of a finished 3D-printed device after bonding can be seen in Figure 1D and a bright-field micrograph showing the channel cross-sectional area in Figure 1E.

The PolyJet printer utilized in this research was manufactured by Stratasys and utilizes proprietary materials. Structures are formed via acrylate cross-linking chemistry using a mixture of acrylate oligomers and monomers along with a photoinitiator.[34]

We first investigated the EOF properties of straight channel devices created from the nichrome wires. Corona discharge is a widely used surface treatment technique for EOF improvements in thermoplastic nanochannels.[39] In theory, the energy of the high-charged electrical corona is believed to break the molecular bonds on the surface of the substrate. The broken bonds then recombine with the free radicals in the corona environment to form additional polar groups on the surface.[40] The EOF of the solution at a pH of 10 (using a boric acid buffer system) in the 3D-printed straight channel devices increased from $2.0 \pm 0.1 \times 10^{-4}$ cm^2/Vs with untreated devices to $3.5 \pm 0.2 \times 10^{-4}$ cm^2/Vs after corona treatment ($n = 4$). A similar EOF value was obtained at pH 11.2 using a CAPS buffer ($3.2 \pm 0.1 \times 10^{-4}$ cm^2/Vs, $n = 3$). Ohm's Law plots were used to further characterize straight channel devices made from 25 and 50 μm nichrome wires. A linear relationship between current and field strength was maintained up to ~750 V/cm for 25 μm dia. channels and 400 V/cm for 50 μm dia. channels. Further increases in electric field strength resulted in current deviating from linearity (Figure S2). These results illustrate that the thermally bonded small channels can tolerate high field strengths before Joule heating occurs. We also attempted to use the embedding wire technique to produce microchannels on separate 3D prints and then fuse the two pieces together to form cross-channels (T-structures). The final devices had channels in different planes; however, the depth at the intersection of the channels was double that of the rest of the channels. This created issues in reproducibility of the volume of sample injected and re-establishment of flow profiles after gated injection.

To create T-channel structures that could be used for gated or pinched injection schemes, various molds were investigated. Figure 2 depicts the stepwise fabrication process of devices with T/cross-channel structure in the same plane, in this example, using a prefabricated brass mold (similar to ones used for hot embossing and injection molding).[29,41] The mold is placed on the print tray, and the tray is dropped by the thickness of the mold and the raised structure. Printing of material (including a reservoir) is done on top of the mold. After printing, the material
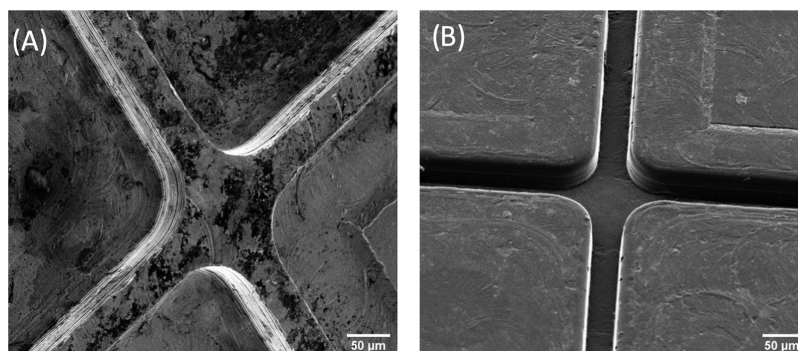
Figure 3. Scanning electron micrograph of (A) positive relief structure on brass mold and (B) cross-channel intersection created from 3D printing on positive relief structure.
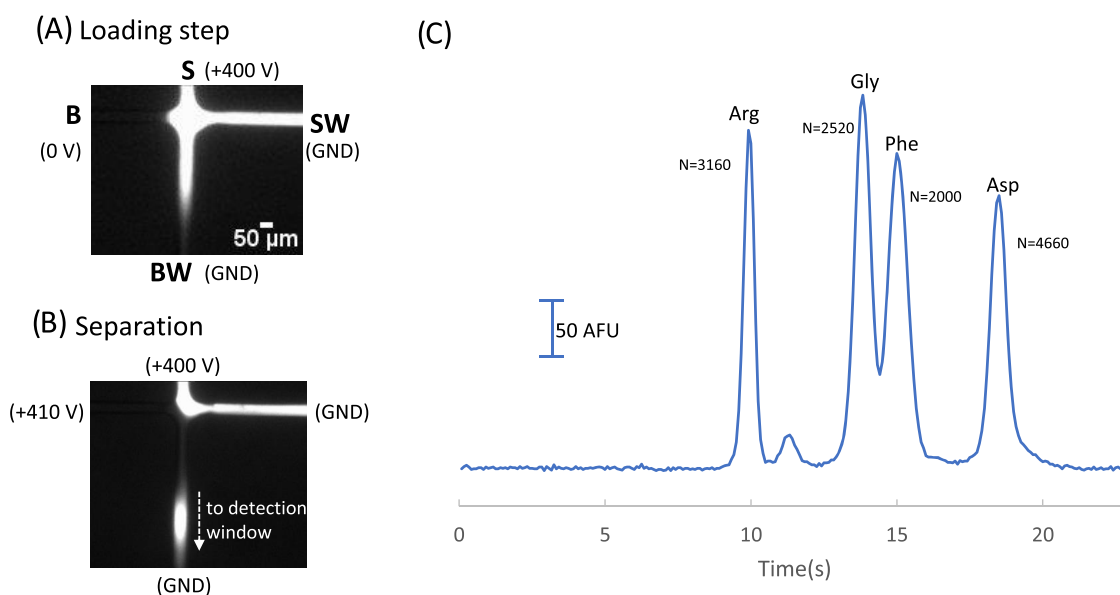

Figure 4. Data obtained from the device printed on a brass mold. Fluorescence micrographs were captured during gating injection including (A) loading step and (B) separation. (C) Electropherogram of a four amino acid mixture that was prelabeled with FITC. The concentration of each amino acid in the injection sample was 200 μM in 20 mM boric acid (pH = 10). The small peak migrating just after Arg was not identified. The running buffer used was 20 mM boric acid (pH = 10), and the field strength was 150 V/cm. An inverted fluorescence microscope was focused on the separation channel 0.70 cm from the injection point for fluorescence detection.

readily delaminates from the mold to leave a negative relief structure. A laser profiler was used to measure the device microchannel dimensions (depth and width), and these were complementary to the positive structure on the brass mold (42 × 42 μm^2). Figure 2D,E shows the bright-field micrograph of the channel intersection before and after bonding. The optimized bonding conditions did not alter the dimensions of channels during bonding. Figure 3A shows the SEM photomicrograph of the microstructures milled in brass. The micromilling process is unable to make sharp inside corners (see Figure 3B) due to the intrinsic feature of the process itself, as seen previously.[29] The size of the milling bit determines the curvature of corners, and at the same time, the achievable height of the structure is limited by the useful flute length of the mill bit.[29]

A gated injection sequence was used to initiate separation of four amino acids labeled with FITC. For the loading step, +400 V was applied at the sample (S) reservoir to direct sample to grounded sample waste (SW) and +410 V at buffer (B) reservoir to grounded buffer waste (BW). To complete an injection into the separation channel, the B reservoir was held at 0 V for 2 s, as shown in Figure 4A. When the buffer voltage was restored,

separation was initiated, and the initial flow profiles were re-established. The plug migration down the separation channel toward the detection window was facilitated by a field strength of 150 V/cm (Figure 4B). The injected plug volume was 0.51 nL. Separations were monitored using a fluorescence microscope and a CCD camera with the detection window being set 0.7 cm from the injection point. Figure 4C shows the electropherogram of the separated FITC-labeled amino acids. The device rapidly resolved the labeled amino acids in less than 20 s with good separation efficiency ranging from 2000 to 4660 theoretical plates. At this field strength, these devices offer comparable separation efficiency to other plastic and 3D-printed microchip electrophoresis devices with similar separation distance and analytes.[27,42] For example, the aforementioned SLA-printed microchip electrophoresis device achieved 1600−1700 theoretical plates for the separation and fluorescence detection of labeled amino acids.[27] To demonstrate the reproducibility and EOF stability, a calibration curve was performed with varying concentrations of an arginine and glycine mixture (100−500 μM). Injections were done in triplicate for each concentration. Figure S3A shows the electropherogram of the two well-
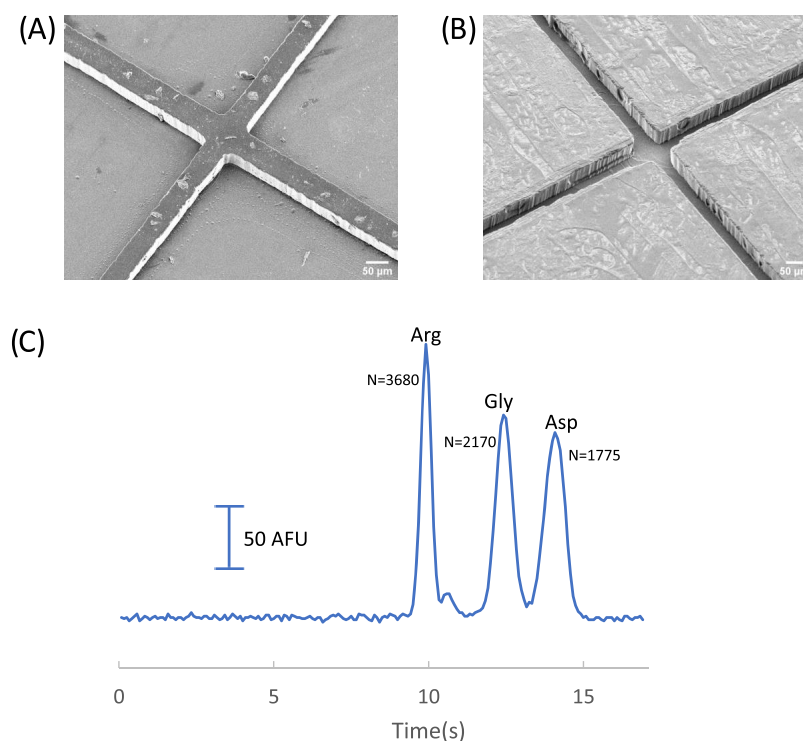
Figure 5. Data obtained from the device printed on a PDMS mold. Scanning electron micrograph of (A) PDMS-based positive relief structure; (B) cross-channel intersection created from 3D printing on PDMS-based positive relief structure; and (C) electropherogram of FITC-labeled amino acids using the device. Electrophoretic conditions: running buffer, 20 mM boric acid (pH = 10); field strength 220 V/cm, detection window 0.65 cm from the injection point.

separated amino acids at each concentration. A linear increase in peak height with concentration is shown in the calibration curve (Figure S3B). Low concentrations of the analyte were not explored because the microscope used in this study used a Hg arc lamp for excitation, as opposed to a laser system. A pinched injection scheme could also be used with this device, and that process is demonstrated in Figure S4.

Other approaches can be used to create molds including less expensive PDMS molds. Positive relief PDMS molds were made with a negative resist and positive photomask. A similar process to Figure 2 was used to make the devices, with the positive relief PDMS mold being placed on the print tray, and the tray was dropped by the thickness of the PDMS and structure. Figure 5A,B shows the SEM micrographs of the positive relief structure made from PDMS and the complementary cross microchannels in the 3D-printed part. The fabricated channel dimensions were $50 \times 50~\mu\mathrm{m}^2$ (width × depth). Devices from PDMS mold had sharp inside corners compared to devices fabricated from brass mold. A mixture of FITC-labeled Arg, Gly, and Asp amino acids were separated by applying a field strength of 220 V/cm down the separation channel. The injected plug volume was 0.52 nL. The number of theoretical plates ranged from 3680 for Arg to 1775 for Asp.

The ability to use a sacrificial material (in this case, carbon ink) with the general approach outlined in Figure 2 was also explored. This process is outlined in Figure 6A−C. A negative relief PDMS structure was sealed to a piece of glass, and a diluted carbon ink mixture was filled into the channel network. Following a drying step and removal of the PDMS mold, the carbon ink structure and glass were placed on the print tray. The tray was dropped by the thickness of the glass and structure and the design printed. When removing the printed part from the

glass, the carbon ink transfers into the part. In mold fabrication, a considerable amount of carbon ink shrinking occurs during drying in the oven, during which time the thin film deviates from the original shape of the PDMS mold. This limits the length of the channels that can be fabricated from this technique to ∼0.4 cm. In our experience, it was difficult to completely remove all of the carbon ink material without deforming the channels of devices when the carbon ink was thicker than 20 μm. Therefore, with this technique, channel dimensions are limited to less than 20 μm in depth. With this approach, we successfully fabricated devices with channel sizes as small as $48 \times 12~\mu\mathrm{m}^2$. Four FITC-labeled amino acids were successfully separated using these devices at 250 V/cm (Figure 6D). Applying these voltages did not cause buffer electrolysis or any bubble formation in the channels during the 20 s analysis time. The separation resolution and efficiency (average of 310 theoretical plates) were not as good as the devices created from the brass or PDMS molds due to the shorter separation distance (0.4 cm total length, detection window only 0.3 cm from the injection point).

■ CONCLUSIONS

In summary, we have shown that the use of commercially available PolyJet 3D printer is fully capable of printing truly microfluidic flow channels when micromolds and sacrificial material are incorporated into the printing process. Straight channels with dimensions as small as 25 μm diameter and T-designs with cross sections as small as $48 \times 12~\mu\mathrm{m}^2$ can be fabricated from this technique. Ohm's Law plots and EOF analysis were performed, and either a gated or pinched injection scheme can be used with the sealed devices. Separation of four amino acids was achieved with up to 4660 theoretical plates. While the use of carbon ink as a sacrificial material resulted in the
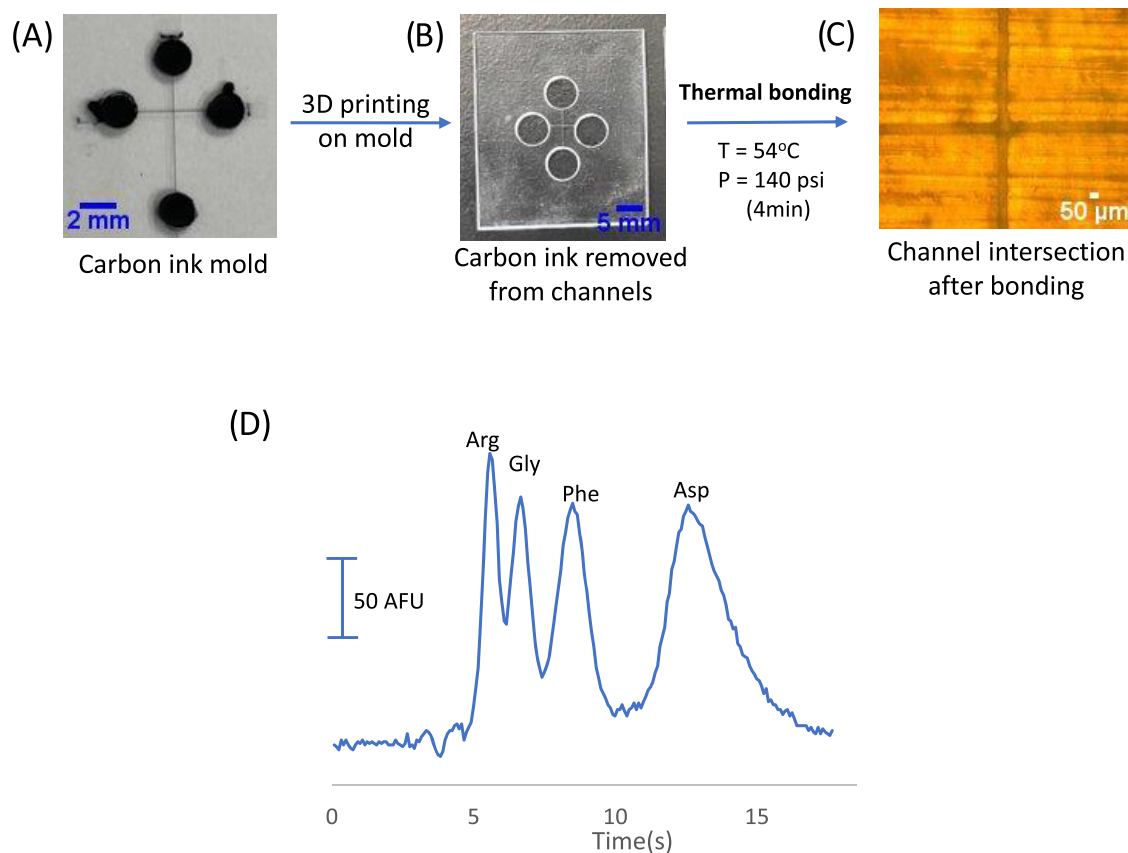
Figure 6. Fabrication of cross-microchannel structure by Polyjet-based 3D printing on sacrificial material (carbon ink). PDMS mold is used to define the carbon ink on a glass surface. After drying, the PDMS is removed (shown in A). The device model is printed on top of the carbon ink microstructure, and the carbon ink material is transferred into the device and removed with a thinner solution. The open-channel structure is shown in (B). (C) Bright-field micrograph of channel intersection after bonding. (D) Electropherogram of FITC-labeled amino acids. The running buffer was 20 mM boric acid (pH = 10), and the detection window was 0.3 cm from the injection point (field strength = 250 V/cm).

fabrication of short channel lengths, there is the opportunity to explore other sacrificial materials that can be easily removed from the printed device. With PolyJet printing, several materials can easily be incorporated into one print.[43,44] Therefore, microchip electrophoresis devices with pumps and valves could be investigated in future work. While this application is focused on microchip electrophoresis, the ability to 3D-print against molds that can subsequently be removed is a general methodology to decrease channel size for other applications and other types of 3D printing as well as to possibly integrate 3D printing with other production processes since we have shown that molds commonly used for hot embossing and injection molding can be incorporated in the stacked printing process.

ASSOCIATED CONTENT

Ⓢ Supporting Information

The Supporting Information is available free of charge at https://pubs.acs.org/doi/10.1021/acsomega.2c01265.

Figure S1 contains (A) a photograph of a 3D-printed device with ridges on the channel layer surface and (B) a photograph of the final device with ridges after thermal bonding; Figure S2 contains Ohm's Law plots for (A) 50 μm (B) 25 μm channel fabricated from the wire mold using a 25 mM boric acid buffer (pH 10); Figure S3 contains (A) electropherograms obtained at different concentrations of FITC-labeled arginine and glycine and (B) corresponding calibration curves for each analyte; and

Figure S4 contains bright-field micrographs of the cross intersection (printed from brass mold) when used for a pinched injection scheme (both the sample loading and injection steps) (PDF)

■ AUTHOR INFORMATION

Corresponding Author

R. Scott Martin − *Department of Chemistry, Saint Louis University, St. Louis, Missouri 63103, United States; Center for Additive Manufacturing, Saint Louis University, Saint Louis, Missouri 63103, United States;* ⊙ orcid.org/0000-0002-6952-1408; Phone: +1 314-977-2836; Email: scott.martin@slu.edu

Authors

Major A. Selemani − *Department of Chemistry, Saint Louis University, St. Louis, Missouri 63103, United States*

Andre D. Castiaux − *Center for Additive Manufacturing, Saint Louis University, Saint Louis, Missouri 63103, United States*

Complete contact information is available at:
https://pubs.acs.org/10.1021/acsomega.2c01265

Notes

The authors declare no competing financial interest.

■ REFERENCES

(1) Lu, N.; Kutter, J. P. Recent advances in microchip enantioseparation and analysis. *Electrophoresis* **2020**, *41*, 2122.

(2) Nuchtavorn, N.; Suntornsuk, W.; Lunte, S. M.; Suntornsuk, L. Recent applications of microchip electrophoresis to biomedical analysis. *J. Pharm. Biomed. Anal.* **2015**, *113*, 72−96.

(3) Schilly, K. M.; Gunawardhana, S. M.; Wijesinghe, M. B.; Lunte, S. M. Biological applications of microchip electrophoresis with amperometric detection: in vivo monitoring and cell analysis. *Anal. Bioanal. Chem.* **2020**, *412*, 6101−6119.

(4) Wuethrich, A.; Quirino, J. P. A decade of microchip electrophoresis for clinical diagnostics − A review of 2008−2017. *Anal. Chim. Acta* **2019**, *1045*, 42−66.

(5) Kim, M.-S.; Cho, S. I.; Lee, K.-N.; Kim, Y.-K. Fabrication of microchip electrophoresis devices and effects of channel surface properties on separation efficiency. *Sens. Actuators, B* **2005**, *107*, 818−824.

(6) Castaño-Álvarez, M.; Fernández-Abedul, M. T.; Costa-García, A.; Agirregabiria, M.; Fernández, L. J.; Ruano-López, J. M.; Barredo-Presa, B. Fabrication of SU-8 based microchip electrophoresis with integrated electrochemical detection for neurotransmitters. *Talanta* **2009**, *80*, 24−30.

(7) Nouwairi, R. L.; O'Connell, K. C.; Gunnoe, L. M.; Landers, J. P. Microchip Electrophoresis for Fluorescence-Based Measurement of Polynucleic Acids: Recent Developments. *Anal. Chem.* **2021**, *93*, 367−387.

(8) Harrison, D. J.; Manz, A.; Fan, Z.; Luedi, H.; Widmer, H. M. Capillary electrophoresis and sample injection systems integrated on a planar glass chip. *Anal. Chem.* **1992**, *64*, 1926−1932.

(9) Manz, A.; Harrison, D. J.; Verpoorte, E. M. J.; Fettinger, J. C.; Paulus, A.; Lüdi, H.; Widmer, H. M. Planar chips technology for miniaturization and integration of separation techniques into monitoring systems: Capillary electrophoresis on a chip. *J. Chromatogr. A* **1992**, *593*, 253−258.

(10) Harrison, D. J.; Fluri, K.; Seiler, K.; Fan, Z.; Effenhauser, C. S.; Manz, A. Micromachining a miniaturized capillary electrophoresis-based chemical analysis system on a chip. *Science* **1993**, *261*, 895−897.

(11) Jacobson, S. C.; Hergenroder, R.; Moore, A. W. J.; Ramsey, J. M. Precolumn reactions with electrophoretic analysis integrated on a microchip. *Anal. Chem.* **1994**, *66*, 4127−4132.

(12) Golozar, M.; Chu, W. K.; Casto, L. D.; McCauley, J.; Butterworth, A. L.; Mathies, R. A. Fabrication of high-quality glass microfluidic devices for bioanalytical and space flight applications. *MethodsX* **2020**, *7*, No. 101043.

(13) He, Y.; Wu, W.; Zhang, T.; Fu, J. Micro structure fabrication with a simplified hot embossing method. *RSC Adv.* **2015**, *5*, 39138−39144.

(14) Tsao, C.-W. Polymer microfluidics: Simple, low-cost fabrication process bridging academic lab research to commercialized production. *Micromachines* **2016**, *7*, 225.

(15) Duffy, D. C.; McDonald, J. C.; Schueller, O. J.; Whitesides, G. M. Rapid Prototyping of Microfluidic Systems in Poly(dimethylsiloxane). *Anal. Chem.* **1998**, *70*, 4974−4984.

(16) McDonald, J. C.; Whitesides, G. M. Poly(dimethylsiloxane) as a material for fabricating microfluidic devices. *Acc. Chem. Res.* **2002**, *35*, 491−499.

(17) Friend, J.; Yeo, L. Fabrication of microfluidic devices using polydimethylsiloxane. *Biomicrofluidics* **2010**, *4*, No. 026502.

(18) Lacher, N. A.; de Rooij, N. F.; Verpoorte, E.; Lunte, S. M. Comparison of the performance characteristics of poly-(dimethylsiloxane) and Pyrex microchip electrophoresis devices for peptide separations. *J. Chromatogr. A* **2003**, *1004*, 225−235.

(19) Ocvirk, G.; Munroe, M.; Tang, T.; Oleschuk, R.; Westra, K.; Harrison, D. J. Electrokinetic control of fluid flow in native poly(dimethylsiloxane) capillary electrophoresis devices. *Electrophoresis* **2000**, *21*, 107−115.

(20) Erkal, J. L.; Selimovic, A.; Gross, B. C.; Lockwood, S. Y.; Walton, E. L.; McNamara, S.; Martin, R. S.; Spence, D. M. 3D printed microfluidic devices with integrated versatile and reusable electrodes. *Lab Chip* **2014**, *14*, 2023−2032.

(21) Anderson, K. B.; Lockwood, S. Y.; Martin, R. S.; Spence, D. M. A 3D Printed Fluidic Device that Enables Integrated Features. *Anal. Chem.* **2013**, *85*, 5622−5626.

(22) Li, F.; Macdonald, N. P.; Guijt, R. M.; Breadmore, M. C. Multimaterial 3D Printed Fluidic Device for Measuring Pharmaceuticals in Biological Fluids. *Anal. Chem.* **2019**, *91*, 1758−1763.

(23) Chen, C.; Mehl, B. T.; Munshi, A. S.; Townsend, A. D.; Spence, D. M.; Martin, R. S. 3D-printed Microfluidic Devices: Fabrication, Advantages and Limitations-a Mini Review. *Anal. Methods* **2016**, *8*, 6005−6012.

(24) Castiaux, A. D.; Currens, E. R.; Martin, R. S. Direct embedding and versatile placement of electrodes in 3D printed microfluidic-devices. *Analyst* **2020**, *145*, 3274−3282.

(25) Preuss, J.-A.; Nguyen, G. N.; Berk, V.; Bahnemann, J. Miniaturized free-flow electrophoresis: production, optimization, and application using 3D printing technology. *Electrophoresis* **2021**, *42*, 305−314.

(26) Gong, H.; Bickham, B. P.; Woolley, A. T.; Nordin, G. P. Custom 3D printer and resin for 18 μm × 20 μm microfluidic flow channels. *Lab Chip* **2017**, *17*, 2899−2909.

(27) Beauchamp, M. J.; Nielsen, A. V.; Gong, H.; Nordin, G. P.; Woolley, A. T. 3D Printed Microfluidic Devices for Microchip Electrophoresis of Preterm Birth Biomarkers. *Anal. Chem.* **2019**, *91*, 7418−7425.

(28) Costa, B. M. C.; Coelho, A. G.; Beauchamp, M. J.; Nielsen, J. B.; Nordin, G. P.; Woolley, A. T.; da Silva, J. A. F. 3D-printed microchip electrophoresis device containing spiral electrodes for integrated capacitively coupled contactless conductivity detection. *Anal. Bioanal. Chem.* **2022**, *414*, 545.

(29) Hupert, M. L.; Guy, W. J.; Llopis, S. D.; Shadpour, H.; Rani, S.; Nikitopoulos, D. E.; Soper, S. A. Evaluation of micromilled metal mold masters for the replication of microchip electrophoresis devices. *Microfluid. Nanofluid.* **2006**, *3*, 1−11.

(30) Kim, E.; Xia, Y.; Whitesides, G. M. Micromolding in Capillaries: Applications in Materials Science. *J. Am. Chem. Soc.* **1996**, *118*, 5722−5731.

(31) Kovarik, M. L.; Torrence, N. J.; Spence, D. M.; Martin, R. S. Fabrication of carbon microelectrodes with a micromolding technique and their use in microchip-based flow analyses. *Analyst* **2004**, *129*, 400−405.

(32) Kuhnline, C. D.; Gangel, M. G.; Hulvey, M. K.; Martin, R. S. Detecting thiols in a microchip device using micromolded carbon ink electrodes modified with cobalt phthalocyanine. *Analyst* **2006**, *131*, 202−207.

(33) Rimington, R. P.; Capel, A. J.; Player, D. J.; Bibb, R. J.; Christie, S. D. R.; Lewis, M. P. Feasibility and Biocompatibility of 3D-Printed Photopolymerized and Laser Sintered Polymers for Neuronal, Myogenic, and Hepatic Cell Types. *Macromol. Biosci.* **2018**, *18*, No. 1800113.

(34) VeroClear RGD810 MSDS; SDS-06119 EN A; Stratasys: Eden Prairie, MN, 2021. https://stratasysstorage01.file.core.windows.net/ssys-websites-files-prod/SDS/Werc/SDS-06119/SDS-06119_29Sep21_American%20English_AGHS_VeroClear_RGD810.pdf?sv=2017-04-17&sr=f&sig=kH%2FV83xqTgQPzDTjmMMOHmvwLA%2BXGrtfvIKE5%2FLbTfQ%3D&st=2022-01-11T15%3A20%3A07Z&se=2023-01-12T15%3A20%3A07Z&sp=rwl (accessed 03/01/2022).

(35) Castiaux, A. D.; Pinger, C. W.; Hayter, E. A.; Bunn, M. E.; Martin, R. S.; Spence, D. M. PolyJet 3D-Printed Enclosed Microfluidic

Channels without Photocurable Supports. *Anal. Chem.* **2019**, *91*, 6910−6917.

(36) Filla, L. A.; Kirkpatrick, D. C.; Martin, R. S. Use of a corona discharge to selectively pattern a hydrophilic/hydrophobic interface for integrating segmented flow with microchip electrophoresis and electrochemical detection. *Anal. Chem.* **2011**, *83*, 5996−6003.

(37) Huang, X.; Gordon, M. J.; Zare, R. N. Current-monitoring method for measuring the electroosmotic flow rate in capillary zone electrophoresis. *Anal. Chem.* **1988**, *60*, 1837−1838.

(38) Kim, B. Y.; Yang, J.; Gong, M.; Flachsbart, B. R.; Shannon, M. A.; Bohn, P. W.; Sweedler, J. V. Multidimensional Separation of Chiral Amino Acid Mixtures in a Multilayered Three-Dimensional Hybrid Microfluidic/Nanofluidic Device. *Anal. Chem.* **2009**, *81*, 2715−2722.

(39) Suzuki, H.; Kasai, K.; Kimura, Y.; Miyata, S. UV/ozone surface modification combined with atmospheric pressure plasma irradiation for cell culture plastics to improve pluripotent stem cell culture. *Mater. Sci. Eng. C* **2021**, *123*, No. 112012.

(40) McKeen, L. W. 11 - Powder Coating and Films. In *Fluorinated Coatings and Finishes Handbook (Second Edition)*,McKeen, L. W., Ed.; William Andrew Publishing: Oxford, 2016; pp 185−209.

(41) Koesdjojo, M. T.; Tennico, Y. H.; Remcho, V. T. Fabrication of a microfluidic system for capillary electrophoresis using a two-stage embossing technique and solvent welding on poly(methyl methacrylate) with water as a sacrificial layer. *Anal. Chem.* **2008**, *80*, 2311−2318.

(42) Kelly, R. T.; Woolley, A. T. Thermal bonding of polymeric capillary electrophoresis microdevices in water. *Anal. Chem.* **2003**, *75*, 1941−1945.

(43) Bowen, A. L.; Martin, R. S. Integration of on-chip peristaltic pumps and injection valves with microchip electrophoresis and electrochemical detection. *Electrophoresis* **2010**, *31*, 2534−2540.

(44) Castiaux, A. D.; Selemani, M. A.; Ward, M. A.; Martin, R. S. Fully 3D printed fluidic devices with integrated valves and pumps for flow injection analysis. *Anal. Methods* **2021**, *13*, 5017.